Science Advances
AAAS

# Supplementary Materials for

## Presynaptic nanoscale components of retrograde synaptic signaling

Benjámin Barti *et al.*

Corresponding author: István Katona, ikatona@iu.edu, katona@koki.hu

*Sci. Adv.* **10**, eado0077 (2024)
DOI: 10.1126/sciadv.ado0077

**The PDF file includes:**

Figs. S1 to S8
Tables S1 and S2
Legend for data S1

**Other Supplementary Material for this manuscript includes the following:**

Data S1

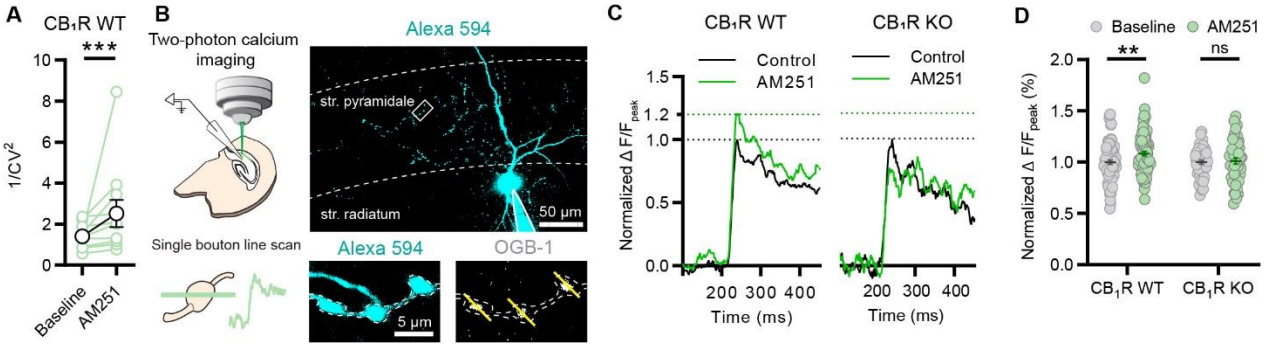


**Fig. S1. Presynaptically located $CB_1$Rs account for the synaptic cannabinoid tone.**

**A)** Comparison of the $1/CV^2$ value of IPSC amplitudes in WT mice before and after AM251 application in paired recordings (n = 11 pairs, ***p = 0.001, Wilcoxon signed-rank test).

**B)** Schematic illustration and representative images of the experimental design of two-photon calcium imaging. $CB_1$BCs visualized by Alexa 594 dye (cyan), calcium transients after evoked action potentials were measured via OGB-1 dye (white). Boxed region enlarged at the bottom shows example boutons sampled with line scans (yellow lines).

**C)** Representative normalized traces of ΔF/F fluorescence measured by line scans in identified perisomatic boutons in $CB_1$R WT and KO samples (n = 20 WT and 23 KO boutons) before and after application of AM251 (10 µM).

**D)** Summary graphs of ΔF/F fluorescence values before and after application of AM251 in $CB_1$R WT (n = 87 boutons from 6 interneurons, **p = 0.002) and in KO boutons (n = 46 boutons from 3 interneurons, $p_{ns}$ = 0.77, Two-way ANOVA with repeated measures).

Graphs show mean ± SEM with individual values.

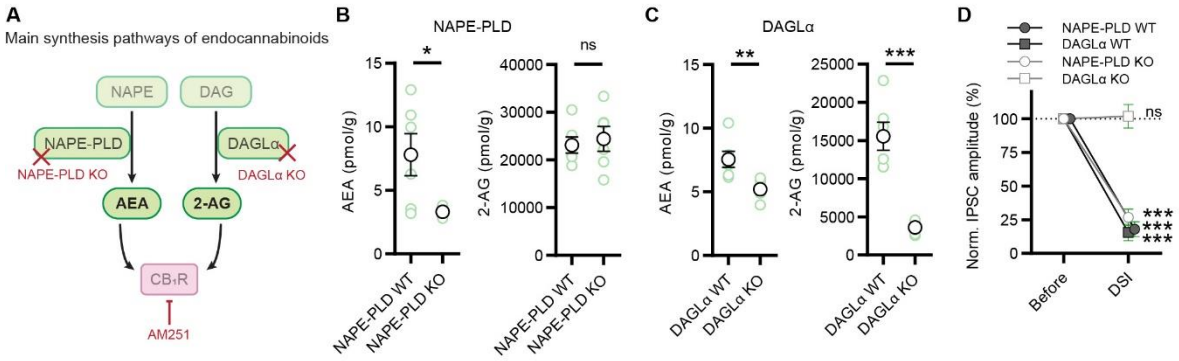


**Fig. S2. Absence of homeostatic compensation of endocannabinoid levels in NAPE-PLD- and DAGLα-knockout mice.**

**A)** Schematic representation of the main biosynthetic pathways of the two endocannabinoid messenger molecules anandamide (AEA) and 2-arachidonoylglycerol (2-AG). The precursor molecules N-acyl-phosphatidylethanolamine (NAPE) and diacylglycerol (DAG) are hydrolyzed by N-acyl-phosphatidylethanolamine-hydrolyzing phospholipase D (NAPE-PLD) and diacylglycerol lipase α (DAGLα), respectively.

**B, C)** Liquid chromatography, tandem mass spectrometry measurement of AEA and 2-AG levels in acute hippocampal slices obtained from **B)** NAPE-PLD WT, KO littermate mice (n = 6 samples/ genotype, *p = 0.0226 in case of AEA, $p_{ns}$ = 0.68 in case of 2-AG, Unpaired t-test) and from **C)** DAGLα WT and KO littermate mice (n = 6 samples/ genotype, **p = 0.007 in case of AEA, ***p < 0.0001 in case of 2-AG, Unpaired t-test).

**D)** Summary graph shows normalized IPSC amplitudes measured in paired recordings before and after induction of depolarization-induced suppression of inhibition (DSI) in NAPE-PLD WT, KO and DAGLα WT, KO samples (NAPE-PLD WT, KO: n = 7 - 7 pairs, DAGLα WT, KO: n = 15 - 11 pairs, ***p < 0.0001; $p_{ns}$ = 0.75; Two-way ANOVA with repeated measures).

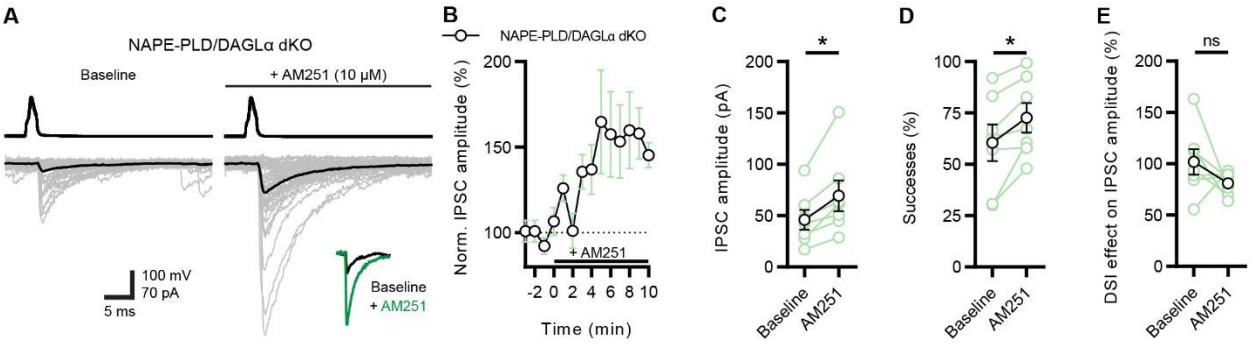


**Fig. S3. Tonic cannabinoid signaling is unaltered in NAPE-PLD/DAGLα dKO mice.**

**A)** Representative traces from paired recordings obtained from NAPE-PLD/DAGLα dKO mice before and after the application of AM251.

**B)** Summary plots of whole experiments show increase of IPSC amplitudes after AM251 application.

**C)** Summary graph of IPSC amplitudes before and after application of AM251 (n = 7 pairs, *p = 0.01).

**D)** Summary graph of successful postsynaptic events (*p = 0.02).

**E)** Summary graph of DSI effect on IPSC amplitude before and after application of AM251 ($p_{ns}$ = 0.2).

Graphs show mean ± SEM with individual values, **C**-**E**: Paired t-test.

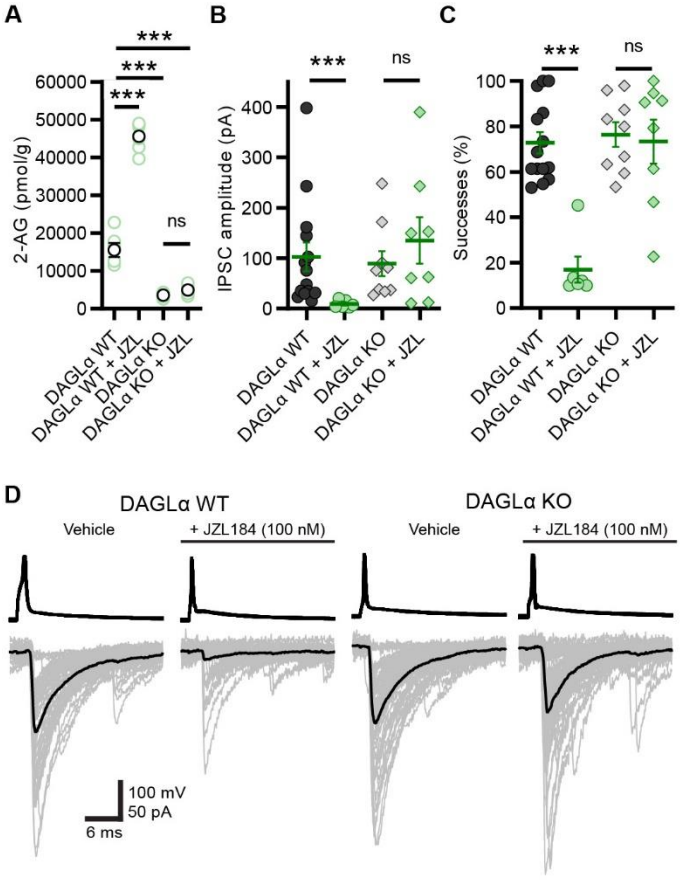


**Fig. S4. DAGL*α*-dependent tonic 2-AG production and synaptic effects are constrained by constitutive MAGL activity.**

**A)** 2-AG lipid measurements of DAGLα WT and KO hippocampal slices after pretreatment with either DMSO (vehicle) or with the irreversible MAGL inhibitor JZL184 (100 nM) for 40 minutes (n = 6 animals/ group, 6 samples/ treatment, ***p < 0.0001, $p_{ns}$ = 0.057, Unpaired t-test).

**B, C)** Summary graphs of electrophysiological experiments obtained from acute slices after 40 min incubation in each condition showed on panel **A**, and effect on IPSC amplitude (**B**) and successes (**C**) in DAGLα KO pairs (WT: n = 14 pairs, WT+JZL184: n = 6 pairs, KO: n = 9 pairs, KO+JZL184: n = 8 pairs, IPSCs amplitude: ***p = 0.0002, $p_{ns}$ = 0.81, successes: ***p < 0.0001, $p_{ns}$ > 0.99, Mann-Whitney U test).

**D)** Example traces of paired recordings from slices incubated in each condition shown above. Graphs show median ± IQR with individual values except on panel **A**, where it shows mean ± SEM with individual values.

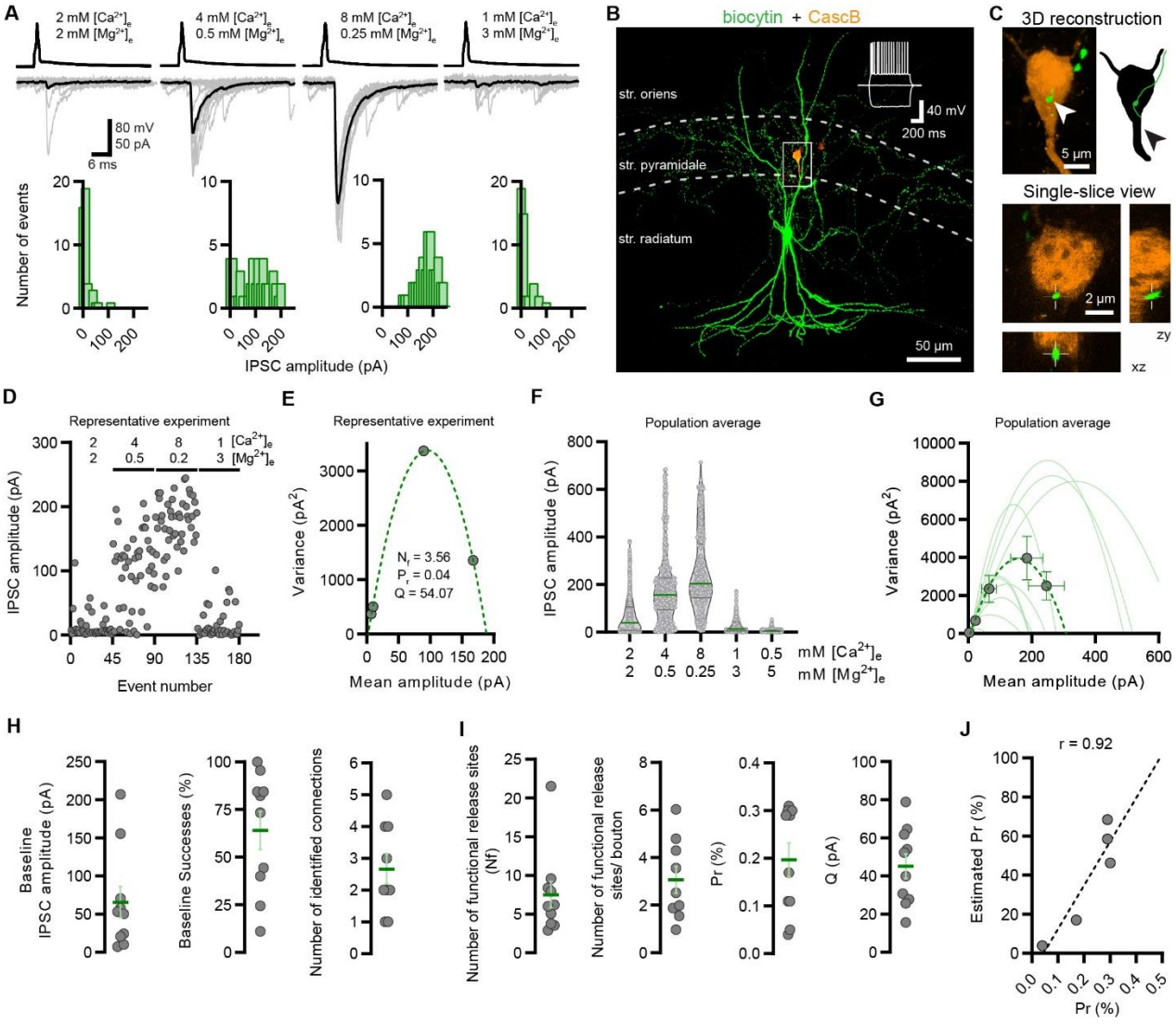


**Fig. S5. Estimation of the quantal properties of synaptic transmission between CB$_1$BC and CA1 pyramidal cells by variance-mean analysis.**

**A)** Variance-mean (V-M) analysis performed on synaptically connected cell pairs: after baseline recordings, Pr was continuously modified via altering the concentration of extracellular $Ca^{2+}$ and $Mg^{2+}$ in the ACSF as shown on representative traces.

**B)** Confocal maximum intensity projection image of the same pair recorded on panel **A**. Inset traces show interneuron responses to -200, 0 and +100 pA current injections.

**C)** High magnification confocal images of boxed region in **B**. 3D view, schematic morphological reconstruction and single-slice view shows single labeled synaptic bouton (arrowhead) on perisomatic region of a postsynaptic pyramidal cell.

**D) P**eak IPSC amplitude in analyzed epochs for the representative experiment shown in **A-C**.

**E)** Parabolic function fitted on the variance–mean amplitude plot reveals quantal parameters such as the number of functional release sites (Nf), the baseline release probability (Pr) and quantal size (Q) obtained during the experiment.

**F)** Plot of peak IPSC amplitude in analyzed epochs for all measured V-M pairs. Violin plots show median ± IQR values with individual data points.

**G)** Summary variance–mean amplitude plot of all V-M experiments (n = 10 pairs). Average population data presented as mean ± SEM.

**H)** Main baseline electrophysiological and anatomical parameters of pairs analyzed in V-M recordings. Data presented as mean ± SEM with individual values.

**I)** Quantal parameters of $CB_1$BC – CA1 pyramidal cell synapses obtained via V-M analysis. Data presented as mean ± SEM with individual values.

**J)** Correlation between measured Pr and estimated Pr in V-M analysis pairs connected with only 1 (n = 2) or 2 (n = 3) boutons (n = 5 pairs, *p = 0.027, r = 0.92, Pearson`s correlation).

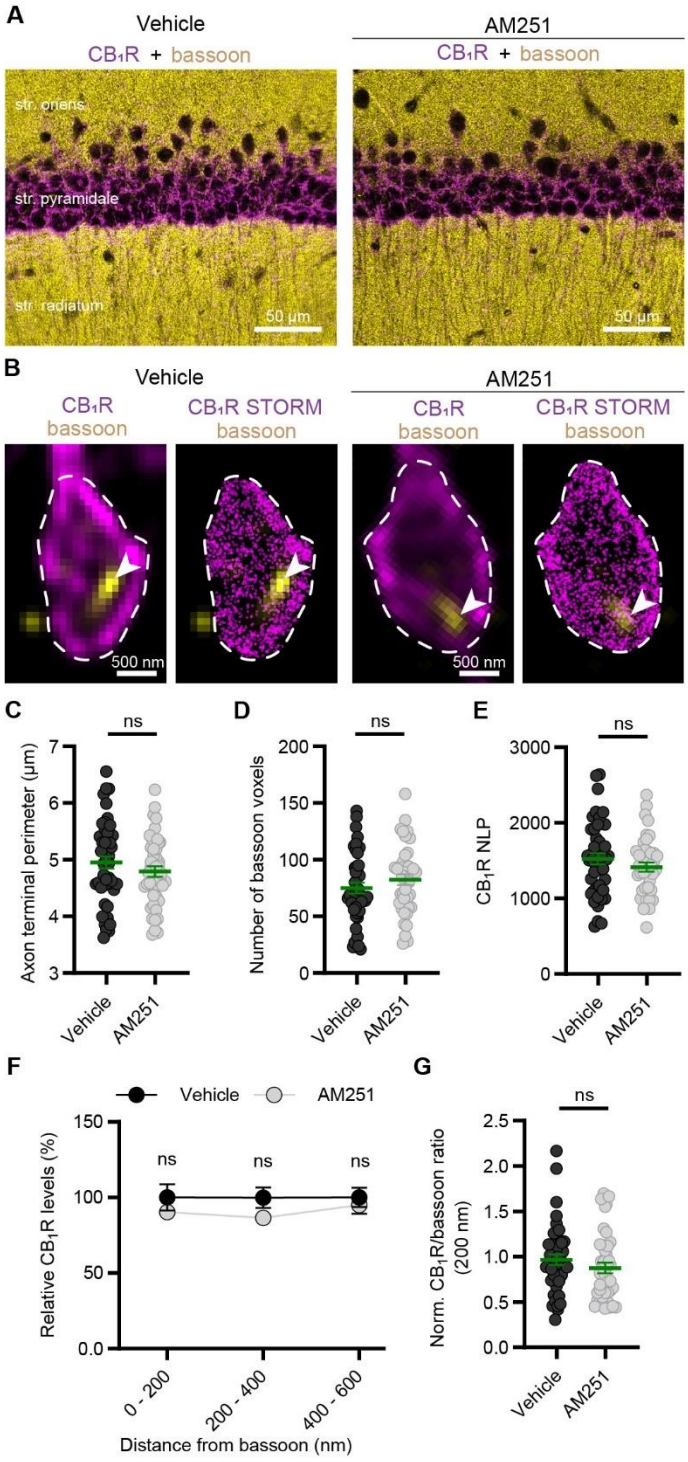


**Fig. S6. AM251 incubation does not influence CB₁R localizations around synaptic active zones.**

**A)** Confocal images of vehicle and AM251 treated slices in the hippocampal CA1 region show immunolabeling for CB₁R (magenta) and bassoon (yellow).

**B)** High-magnification confocal images and corresponding STORM super-resolution images of vehicle and AM251 treated boutons in the pyramidal layer

**C)** Summary graph of the perimeter of axon terminals in vehicle and AM251 treated samples (VEH: n = 46 boutons, AM: n = 45 boutons, $p_{ns} = 0.26$).
**D)** Summary graph of the number of bassoon-positive voxels shows identical active zone size in the axon terminals (VEH: n = 45 boutons, AM: n = 42 boutons, $p_{ns} = 0.27$).
**E)** Summary graph of the total number of $CB_1R$ localization points (NLP) on axon terminals measured with STORM ($p_{ns} = 0.25$).
**F)** Summary graph of distance-dependent localization of $CB_1Rs$ on boutons (0-200 nm: $p_{ns} = 0.93$, 200-400 $p_{ns} = 0.27$, 400-600 nm: $p_{ns} = 0.98$).
**G)** Summary graph of nanoscale $CB_1R$/bassoon ratio in the vicinity (200 nm) of the active zone ($p_{ns} = 0.19$).
Graphs show mean ± SEM with individual values, **C-E**: Unpaired t test, **F-G**: Mann-Whitney U test.

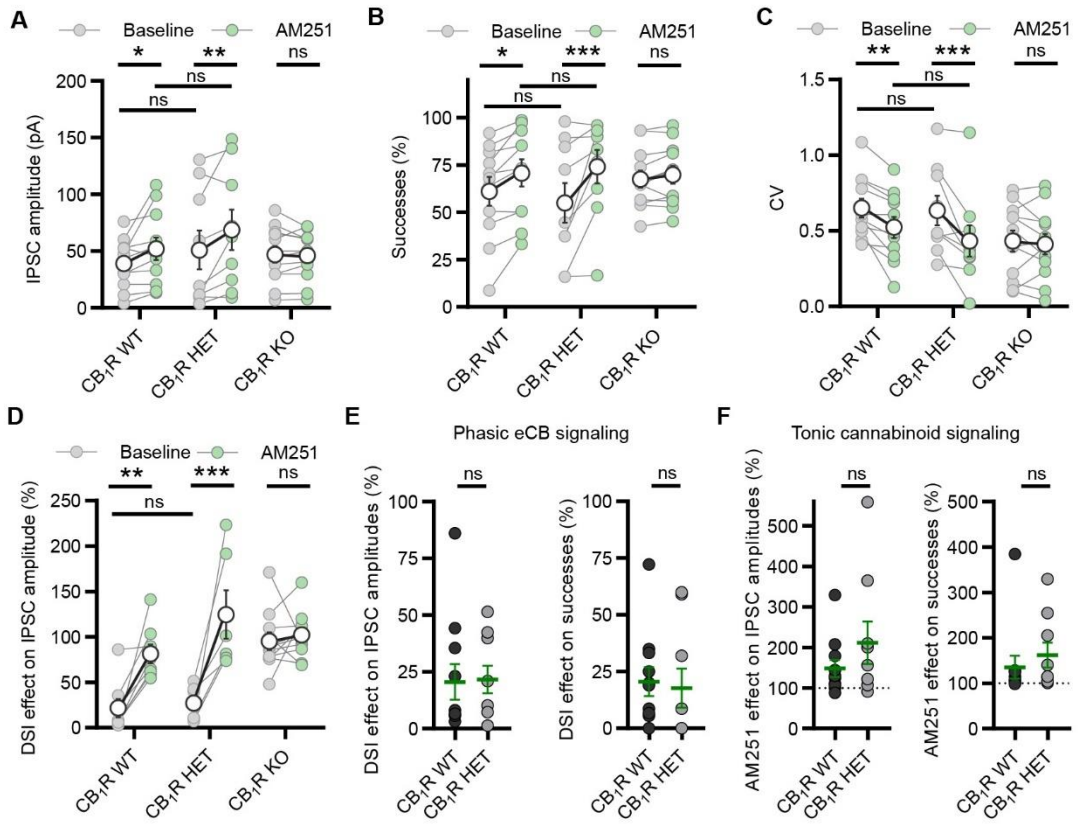


**Fig. S7. $CB_1R$ heterozygous mice do not exhibit changes in phasic endocannabinoid signaling and synaptic cannabinoid tone compared to wild-type mice.**

**A)** Graph of IPSC amplitudes before (baseline) and after application of AM251 in $CB_1R$ WT (n = 11 pairs, *p = 0.01), HET (n = 9 pairs, **p = 0.003) and KO samples (n = 12 pairs, $p_{ns}$ = 0.9).

**B)** Graph of successes before and after application of AM251 in $CB_1R$ WT (*p=0.02), HET (*** p < 0.0001) and KO samples ($p_{ns}$ = 0.5).

**C)** Graph of CV before and after application of AM251 in $CB_1R$ WT (**p=0.004), HET (*** p = 0.0001) and KO samples ($p_{ns}$ = 0.6).

**D)** Summary graph of DSI effect on IPSC amplitudes during baseline and after AM251 application in $CB_1R$ WT (n = 8 pairs, **p=0.001), HET (n = 6 pairs, *** p < 0.0001) and KO samples (n = 11 pairs, $p_{ns}$ = 0.6).

**E)** Effect of DSI (a form of phasic endocannabinoid release) on IPSC amplitudes and successes between $CB_1R$ WT and HET genotypes (WT: n = 11, HET n = 9 pairs, IPSC: $p_{ns}$ = 0.3702, successes: $p_{ns}$ = 0.3696).

**F)** Summary graphs of AM251 effect (unmasked tonic cannabinoid signaling) on baseline IPSC amplitudes and successes in $CB_1R$ WT and HET animals (IPSC: $p_{ns} = 0.5$, successes: $p_{ns} = 0.66$).

Graphs **A-D** shows mean ± SEM with individual values, Two-way ANOVA with repeated measures, **E-F** show median ± IQR with individual values, Mann-Whitney U test.

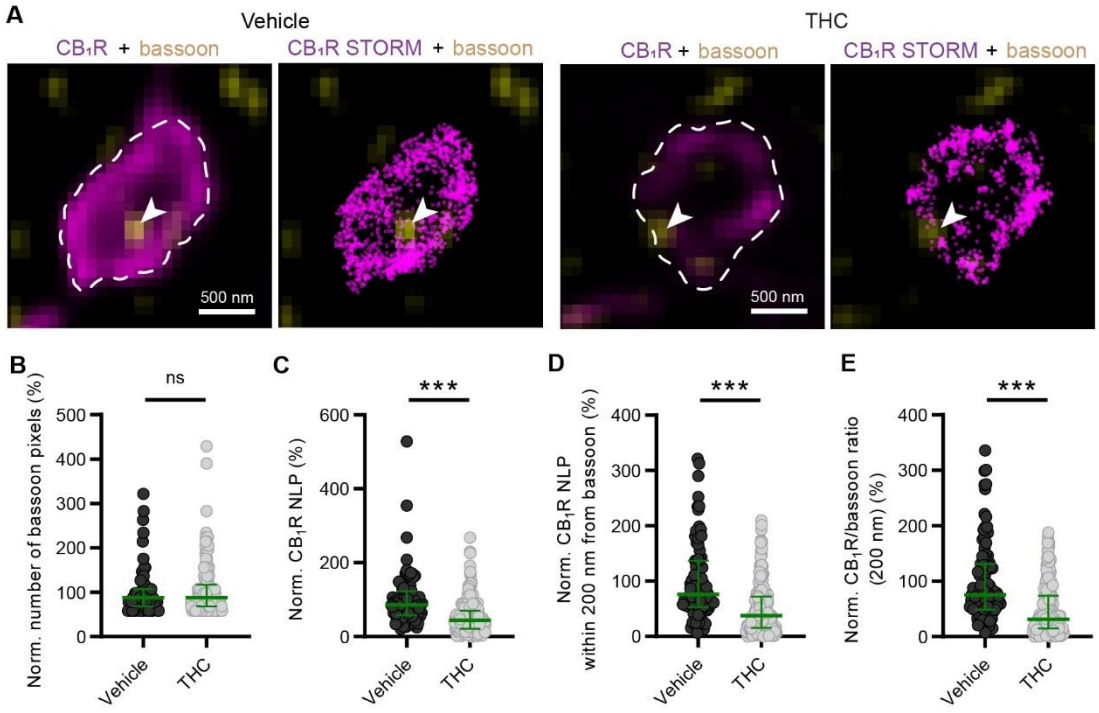


**Fig. S8. In vivo THC treatment disrupts the presynaptic nanoscale receptor/effector ratio in CB$_1$R-positive GABAergic boutons in the CA3 area.**

**A)** Representative confocal- and combined STORM super-resolution images of CB$_1$R immunofluorescent labeling (magenta) on hippocampal GABAergic boutons from either vehicle or THC treated animal groups. Arrowhead marks the synaptic active zone represented by bassoon immunofluorescent staining (yellow).

**B)** Summary graph of the number of bassoon-positive pixels in axon terminals (vehicle: n = 91 boutons, THC: n = 233 boutons, $p_{ns} = 0.95$).

**C)** Summary graph of the total number of CB$_1$R localization points (NLP) on axon terminals measured with STORM (***$p < 0.0001$).

**D)** Summary graph of the number of intra/perisynaptic CB$_1$R localization points (NLP) within 200 nm of the active zone (***$p < 0.0001$).

**E)** Summary graph of CB$_1$R/bassoon ratio between vehicle and THC treated axon terminals (***$p < 0.0001$, Mann-Whitney U test).

Graphs show median ± IQR with individual values.

**Table S1.**

Primary antibodies utilized in the study.

| Antigen | Host species | Dilution | Catalogue number or reference | RRID |
|---|---|---|---|---|
| AF-405/Cascade Blue | Rabbit | 1:1000 | A-5760, Thermo Fisher Scientific (Waltham, USA) | AB_2536192 |
| Bassoon | Mouse | 1:2000 | Ab82958, Abcam (Cambridge, UK) | AB_1860018 |
| $CB_1$ | Guinea pig | 1:2000 | Gift of M. Watanabe (Hokkaido, Japan) | n.a. |
| Parvalbumin | Goat | 1:4000 | PVG-214, Swant (Marly, Switzerland) | AB_10000345 |

**Table S2.**

Fluorescent secondary antibodies utilized in the study.

| Target species | Host species | Dilution | Catalogue number, provider | RRID |
|---|---|---|---|---|
| - (anti-biotin Alexa Fluor/AF 488) | - (Streptavidin) | 1:1000 | 016-540-084, Jackson ImmunoResearch (West Grove, USA) | n.a. |
| anti-goat AF-647 | Donkey | 1:400 | 705-605-147, Jackson | AB_2340437 |
| anti-guinea pig AF-647 | Donkey | 1:1000 | 706-605-148, Jackson | AB_2340476 |
| anti-guinea pig CF-568 | Donkey | 1:1000 | 20377, Biotium (Fremont, USA) | AB_2934264 |
| anti-mouse CF-568 | Donkey | 1:400 | 20105, Biotium | AB_10853136 |
| anti-rabbit DyLight-405 | Donkey | 1:200 | 711-475-152, Jackson | AB_2340616 |

**Data S1. (separate file)**
Source data for manuscript Figs (.xlsx).